NANO LETTERS

pubs.acs.org/NanoLett Letter

High-Pressure Polymerization of Phenol toward Degree-4 Carbon Nanothread

Xin Yang, Guangwei Che, Yajie Wang, Peijie Zhang, Xingyu Tang, Puyi Lang, Dexiang Gao, Xuan Wang, Yida Wang, Takanori Hattori, Jun Abe, Aijiao Guan, Junfeng Xiang, Qian Li, Xiaohuan Lin, Xiao Dong, Ho-kwang Mao, Haiyan Zheng, and Kuo Li*

Cite This: *Nano Lett.* 2025, 25, 1028−1035 Read Online

ACCESS | Metrics & More | Article Recommendations | Supporting Information

ABSTRACT: Saturated sp^3-carbon nanothreads (CNTh) have garnered significant interest due to their predicted high Young's modulus and thermal conductivity. While the incorporation of heteroatoms into the central ring has been shown to influence the formation of CNTh and yield chemically homogeneous products, the impact of pendant groups on the polymerization process remains underexplored. In this study, we investigate the pressure-induced polymerization of phenol, revealing two phase transitions occurring below 0.5 and 4 GPa. Above 20 GPa, phenol polymerizes into degree-4 CNTh featuring hydroxyl and carbonyl groups. Hydrogen transfer of hydroxyl groups was found to hinder the formation of degree-6 nanothreads. Our findings highlight the crucial role of the hydroxyl group in halting further intracolumn polymerization and offer valuable insights for future mechanism research and nanomaterial synthesis.

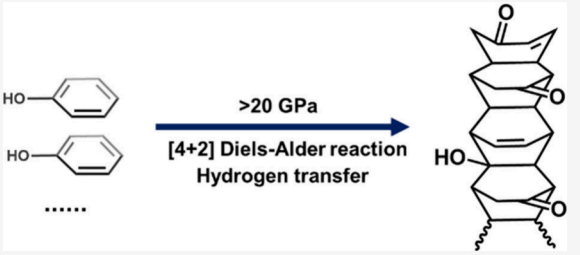

KEYWORDS: *Pressure-induced polymerization, Nanothread, Phenol, Hydrogen transfer*

sp^3-Carbon nanothreads (CNTh) are one-dimensional polymeric nanomaterials characterized by multiple σ-bonds between repeating units. With subnanometer widths and diamond-like tetrahedral local structures, they exhibit high stiffness and flexibility, making them promising candidates for applications such as resonators and reinforcement for nanocomposites.[1,2] These fully saturated (degree-6, indicating six sp^3 carbon atoms on each six-membered ring) C−H polymers were first predicted through theoretical calculations and experimentally confirmed in 2015 by slowly compressing benzene to pressures of up to 20 GPa.[3−7] This demonstrates the effect of high pressure on unsaturated molecular precursors.[8] As intermolecular distances are progressively reduced, π bonds break to form σ bonds between molecules, extending and finally creating one-dimensional nanothread structures. Subsequent research successfully synthesized various CNTh with similar saturated structures from compounds such as furan,[9−12] *s*-triazine,[13] thiophene,[14] and pyridazine.[15] These studies revealed that the incorporation of heteroatoms into the central ring system can guide nanothread formation, enabling the production of chemically homogeneous CNTh.

In contrast, the role of pendant groups in nanothread formation is not fully understood. For example, the introduction of reactive groups like alkynyls onto the aromatic ring can reduce the reaction pressure, though their presence may result in products distinct from typical CNTh, such as carbon nanoribbons synthesized from 1,3,5-triethynylbenzene.[16−18] Fluorine atoms, on the other hand, can enhance the stacking between aromatic and fluorinated aromatic molecules, and by compressing the polycyclic-arene-perfluoroarene, including the naphthalene/octafluoronaphthalene, and anthracene/octafluoronaphthalene, the CNTh products with potentially improving crystallization are obtained.[19−21] However, 1:1 benzene/hexafluorobenzene cocrystal, the smallest arene-perfluoroarene cocrystal, undergoes several complex phase transitions under high pressure and polymerizes into a graphane-type polymer structure rather than CNTh.[22] Studies on aniline suggest that strong hydrogen bonds between $-NH_2$ groups inhibit polymerization up to 30 GPa.[23] Under extreme conditions of 33 GPa and 550 K, a polyaniline-like nanothread was formed, with the $-NH_2$ groups remaining inactive in the reaction.[24] Conversely, Gerthoffer et al. observed the formation of C=O bonds when compressing the phenol-pentafluorophenol cocrystal, indicating the potential involvement of −OH groups in the polymerization process.[21]

Here, we investigated the phase transitions and reactions of phenol under high pressure using Raman, infrared (IR), and

Received: October 2, 2024
Revised: December 19, 2024
Accepted: January 6, 2025
Published: January 10, 2025

https://doi.org/10.1021/acs.nanolett.4c04895
Nano Lett. 2025, 25, 1028−1035

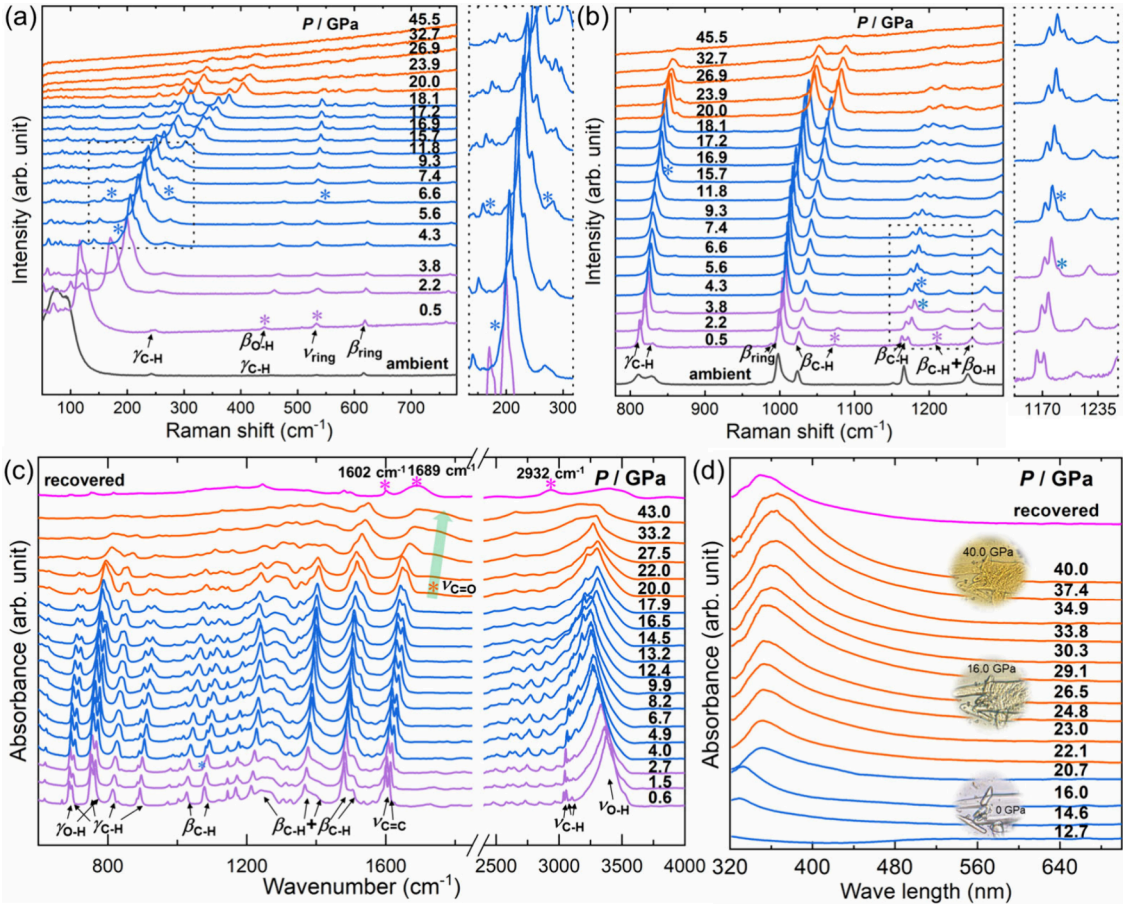

Figure 1. Selected in situ Raman spectra of phenol upon compression in the spectral region of (a) 50−780 cm^{-1} and (b) 780−1300 cm^{-1}. The insets show an enlarged view inside the dashed boxes. (c) Selected in situ IR spectra and (d) in situ UV−vis spectra of phenol under high pressure. The asterisks represent the appearance of new peaks. The green arrow highlights the emerging C=O vibration. The insets show optical images of phenol upon compression.

ultraviolet−visible (UV−vis) spectroscopy; X-ray diffraction (XRD); and neutron diffraction. At pressures above 20 GPa, phenol polymerized into a degree-4 (indicating four sp^3 carbon atoms on each six-membered ring) nanothread, rather than the more common degree-6 nanothread, as confirmed by mass spectrometry and solid-state nuclear magnetic resonance (ssNMR). This polymerization was marked by the formation of new carbonyl groups (C=O), which inhibited further intracolumn polymerization and the development of products with a higher polymerization degree. Our study offers valuable insights into the role of pendant functional groups in CNTh formation and provides a framework for controlling the reactivity of the central ring system and the extent of polymerization under high pressure.

HIGH-PRESSURE PHASE TRANSITION AND REACTION DISCLOSED BY IN SITU SPECTROSCOPY

To track the polymerization process, we independently collected in situ Raman, IR, and UV−vis absorbance spectra. Phenol was rapidly compressed to 0.5 GPa, and the Raman spectra show the features of Phase II (Figure 1a,b and Figure S1), which is consistent with the reported phase transition from the ambient monoclinic phase (Phase I) to Phase II above 0.16 GPa.[25] The Raman mode assignments for Phase II at 0.5 GPa are detailed in Table S1 based on theoretical calculation, and the peaks below 150 cm^{-1} are attributed to lattice phonon vibrations. At 3.8 GPa, a new peak at 1189 cm^{-1} appeared, followed by the appearance of two peaks at 190 and 1185 cm^{-1} at 4.3 GPa. At 6.6 GPa, three additional peaks emerged at 169, 275, and 542 cm^{-1}. These spectral changes suggest another phase transition (Phase II to Phase III). This transition is also indicated by slight discontinuities in the pressure dependence of the Raman shifts (Figure S2). Above 20 GPa, an increase in fluorescence background and degradation of Raman peaks suggest a chemical reaction,[21] which is supported by the subsequent in situ IR spectral results. After decompression from 45.5 GPa to ambient conditions, no Raman peaks were observed against a photoluminescent background (Figure S3), indicating an irreversible reaction.

In situ IR experiments up to 43 GPa (Figure 1c) further confirmed these findings, with the IR peak assignments listed in Table S1. Upon compression, the dependence of IR modes on pressure shows slight discontinuity at ∼4 GPa (Figure S4), and the C−H in-plane bending vibration peak (β_{C-H}, 1078 cm^{-1}) splits at 2.7 GPa, marking the phase transition from Phase II to Phase III. The O−H vibration mode exhibited complex variations: a gradual redshift up to 13.2 GPa, indicating enhanced hydrogen bonding, followed by an abrupt blueshift and a slower blueshift rate up to 20 GPa. Above 20 GPa, the O−H vibration mode redshifts again and a new shoulder peak at 1722 cm^{-1}, attributed to the C=O vibration,

https://doi.org/10.1021/acs.nanolett.4c04895
Nano Lett. 2025, 25, 1028−1035

appears near the C=C vibration. In situ tracking shows the new C=O peak merging with C=C as pressure increased and then separating during decompression (Figure S5). After quenching to ambient pressure and keeping the cell closed (Figure S5 and Figure 1c), the peaks shifted to 1689 and 1602 cm^{-1}, corresponding to C=O and C=C vibrations, respectively, with a new sp^3 C−H peak appearing at 2932 cm^{-1}. This indicates that the C=O peak formed in situ during polymerization. Similar C=O vibration was also detected in the pressure-induced polymerization products of other molecules containing C−O bonds, such as furan and the 1:1 phenol-pentafluorophenol cocrystal etc.[9,21,26] In furan, only a very small amount of C=O (0.3%) was observed, which is claimed to be attributed to a possible ring-opening reaction.[9,10] In contrast, our in situ IR results indicate that carbonyl group formation accompanies polymerization. This may be due to the stability of the keto structure in aliphatic compounds when benzene ring conjugation is disrupted, leading to hydroxyl groups adjacent to unreacted double bonds converting to keto groups.[21] Our finding also suggests that, unlike the amine group in aniline,[24] the hydroxyl group actively participates in the reaction at high pressure and may influence the structure of the final polymerization product.

High-pressure UV−vis absorbance spectra of phenol were measured at up to 40 GPa (Figure 1d) to characterize this reaction. Below 12.7 GPa, the absorption peaks were not detectable due to the limitation of the spectral range of the instrument. At 14.6 GPa, a peak appeared at 329 nm, corresponding to the red-shifted B band ($\pi \rightarrow \pi^*$). This is attributed to the compression of the crystal, which reduces the distance between benzene rings and enhances intermolecular interactions, similar to what occurs in benzene, aniline, and *sym*-heptaphenylcycloheptatriene.[23,27,28] Around 20.7 GPa, this absorption peak underwent a discontinuous red-shift, suggesting the discontinuous variation of optical bandgap, signaling the onset of polymerization (Figure S6a,b). Upon decompression to ambient conditions (Figure S6c), a peak centered at 350 nm was detected in the recovered sample, with an optical band gap of 3.12 eV (Figure S6d), significantly lower than the predicted value for fully saturated benzene CNThs (>4.0 eV), suggesting the presence of sp^2-C defects.[29]

CRYSTAL STRUCTURES UNDER HIGH PRESSURE

To examine the crystal structure evolution of phenol under high pressure, we conducted in situ time-of-flight (TOF) neutron diffraction measurements on full deuterated phenol (phenol-D_6, C_6D_6O) at up to 20 GPa (Figure 2a). To avoid melting, the sample was rapidly compressed to 1 GPa after loading, and the diffraction pattern demonstrates that phenol had transformed to Phase II, as confirmed by Rietveld refinement (Figure S7a). With increasing pressure, all diffraction peaks shifted to lower *d*-values, consistent with gradual lattice compression. Lattice parameters were extracted by Rietveld refinements, revealing anisotropic compression of the crystal from 1 to 20 GPa (Figure S8), with the *a*-axis contracting by 19.9%, the *b*-axis by 9.0%, and the *c*-axis by 7.8%. The pressure−volume (*P*−*V*) relationship was then fitted using the Vinet equation of state (EOS).[30] As shown in Figure 2b, the data between 1 and 20 GPa fit well with the Vinet EOS. Rietveld refinement combined with theoretical optimization (Figure S7 and Tables S2−S4) confirms that the phase transition from Phase II to Phase III observed in Raman

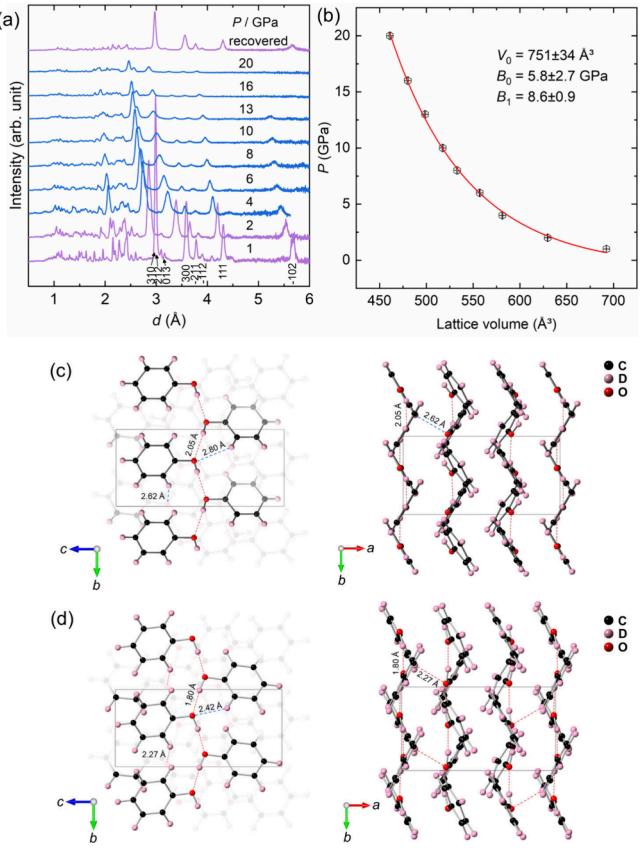

Figure 2. High-pressure crystallographic investigation of phenol. (a) In situ TOF neutron diffraction patterns of phenol up to 20 GPa. (b) Fitting of the Vinet equation of the state of phenol under high pressure in the 1−20 GPa region. The error bars are smaller than the symbols. (c) The crystal structure of phenol Phase II at 1 GPa. The molecules adopt chain structures with hydrogen bonds. (d) The optimized crystal structure of phenol Phase III at 4 GPa with the fixed lattice parameters based on Rietveld refinement result.

and IR spectra is associated with changes in hydrogen bonding without obvious alteration of the bulk modulus.

At 1 GPa in Phase II, the molecules connect via O−H···O hydrogen bonds, extending along the *b*-axis with chain structures (Figure 2c).[25] Within the lattice, four molecular chains are present, which are stacked along the *a*-axis. The shortest C−H···O distance measured between the chains is 2.62 Å. In contrast, the structure of phenol at 4 GPa, which was obtained by optimization with the fixed lattice parameters based on the Rietveld refinement result, reveals that these molecular chains remain aligned along the *b*-axis with a slight change in the O−H···O distance, while the C−H···O distance within the chains decreases to 2.42 Å. Additionally, the distance between chains along the *a*-axis is significantly compressed, with the closest C−H···O distance reducing to 2.27 Å, indicating stronger intermolecular interactions (Figure 2d). This occurs because the molecules form dense stacking chain structures with O−H···O hydrogen bonds on the *b*−*c* plane in Phase II, while the intermolecular interactions along the *a*-axis is weaker, making the interlayer compression along the *a*-axis easier. Consequently, this Phase II to Phase III transition is primarily related to subtle changes in intermolecular forces and molecular stacking along the *a*-axis, rather than molecular rearrangement, and therefore does not result in an abrupt volume change in the *P*−*V* curve. Upon releasing the

https://doi.org/10.1021/acs.nanolett.4c04895
Nano Lett. 2025, 25, 1028−1035

pressure from 20 GPa to ambient pressure, the neutron diffraction pattern reverted without new peaks.

STRUCTURE OF PRODUCT

In comparison to neutron diffraction, the small beam size and specific sample orientation employed in XRD experiments pose challenges in accurately determining the crystal structure by Rietveld refinement. However, it is suitable for achieving a higher pressure and acquiring product diffraction patterns. Thus, we conducted in situ XRD experiments and characterized the recovered sample. At an initial pressure of 1.2 GPa, the sample exhibited a diffraction pattern characteristic of Phase II (Figure S9). With compression, all diffraction peaks shifted toward higher angles (Figure 3a). Above 12.9 GPa,

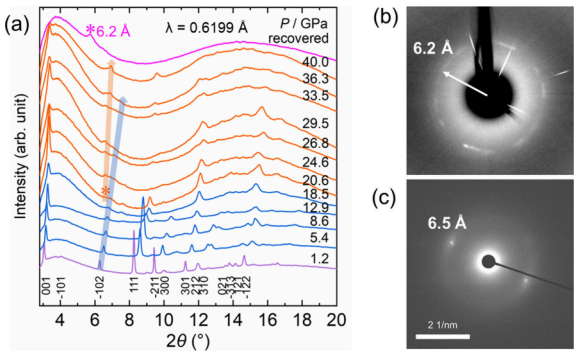

Figure 3. (a) In situ high-pressure XRD data of phenol. The new peaks are marked with asterisks. (b) X-ray diffraction and (c) selected area electron diffraction patterns of the product.

several diffraction peaks began to weaken and eventually disappeared. At 20.6 GPa, a shoulder peak appeared on the low-angle side of the −102 peak, indicating the formation of a reaction product. After being released from 40 GPa to ambient pressure (Figure S10), this new product peak shifted to 6.2 Å, while all phenol peaks vanished (Figure 3b). This irreversible transformation suggests the formation of a low-crystalline product as a result of the high-pressure reaction.

To investigate the structure of the product formed under high pressure, we synthesized several milligrams of the product using a Paris−Edinburg press (PE press) at 30 GPa (PE-30). We then characterized the PE-30 product. The scanning electron microscopy (SEM) image presents a one-dimensional extension of stacked CNThs (Figure S11). The XRD pattern revealed a broad peak centered at 6.2 Å (Figure S12), consistent with the in situ XRD result. Selected area electron diffraction (SAED) further supported this (Figure 3c), displaying diffraction dots at 6.5 Å (the TEM typically has an uncertainty of ∼5% in length scale), corresponding to the spacing between planes of the resulting parallelly stacked nanothreads, similar to previously reported findings.[13,31]

To verify the reaction mechanism, we analyzed the oligomers using electron spray ionization mass spectrometry (ESI-MS). For direct identification of signals from the sample, we used an isotopically labeled sample recovered from the PE press at 30 GPa (PE-30-$^{13}C_6$). Soluble oligomers were extracted by methanol and directly injected into ESI-MS without chromatographic separation. As depicted in Figure 4a, we identified unreacted phenol and major oligomers. From dimer to decamer, a series of product peaks ($^{13}C_{6n}H_{6n-1}O_n$, n = 2, 3, ...) were detected. This mass spectral distribution, separated by individual precursor molecules, resembles findings in the polymerization products of furan,[9] confirming the formation of a 1D thread polymer. Considering the results of furan and phenol:pentafluorophenol cocrystal,[9,21] it is likely that phenol underwent a similar [4 + 2] reaction route. Notably, $^{13}C_{12}H_9O_2$ was also detected as another type of dimer, suggesting the occurrence of side reactions such as 1−1′ coupling.[22] However, no such products of 1−1′ coupling were detected in trimers or higher oligomers. This suggests that the 1−1′ coupling is not the dominant reaction in the generation of the CNTh product.

Solid-state nuclear magnetic resonance (ssNMR) data provide further insights into the insoluble product. After washing away the unreacted phenol with ethanol, the ^{13}C direct polarization (DP) NMR of PE-30-$^{13}C_6$ (Figure 4b) reveals the presence of four types of carbon in the product: C=O (212.8 and 199.8 ppm), C=C (156.3,130.2, and 117.7 ppm), R_3C-O (79.4 ppm), and $C-R_4$ (47.4 and 39.9 ppm). This proves the formation of C=O in the product, consistent with results from IR spectra and X-ray photoelectron spectroscopy (XPS, Figure S13 and Table S5). A fitting analysis was conducted on the DP data to accurately quantify the relative content of each type of carbon subsequently (Figure 4b and Table S6).[32−34] The results show that a significant portion (59.4%) of hydroxyl groups had converted to carbonyl groups, and ∼64.2% of the aromatic carbons had transformed into sp^3 carbons, indicating that each phenol molecule underwent two [4 + 2] cycloaddition reactions on average (involving four carbon atoms). The amount of carbonyl groups present in our product (10.7%) is notably higher than that found in furan CNTh (0.3%).[10] This observation, coupled with the in situ IR results, indicates that the mechanism of carbonyl group formation differs significantly between phenol and furan CNThs. It is also noteworthy that the degree of sp^3 conversion of phenol (64.2%, under 30 GPa) is lower compared to benzene (72%, under 23 GPa),[35] suggesting that the hydroxyl group reduces the reactivity of the benzene ring. This deduction is also supported by residual C=C double bonds detected in the IR of phenol and pentafluorophenol cocrystal polymerization products.[21]

To elucidate the local structure from the NMR results, we simulated the chemical shifts of all possible local structures with polymerization degrees of VI, IV, and II (PD-VI, IV, and II; Figure 4c). Here, PD-VI signifies six carbon atoms of each ring forming new σ bonds with neighbored rings, while PD-IV and II represent four and two carbon atoms forming new σ bonds, respectively. After comparison with the experimental data, we did not observe a significant R_3C-O peak at 64 ppm, suggesting that PD-VI units are absent under current instrumental sensitivity. However, all three types of PD-IV units appear to be present in the product, with PD-IV-1 and -2 carrying −OH and PD-IV-3 carrying C=O. Regarding PD-II units, we identified PD-II-3 based on the peak at 156.3 ppm, as it is the only structure predicted to have a chemical shift of 158.8 ppm.

Given that the average sp^3 carbon content of the product is 64.2%, this indicates an approximate ratio of PD-IV units (with 66.6% sp^3-C) to PD-II units (with 33.3% sp^3-C) in the product of roughly 9:1. Based on this ratio, we assumed some decamer models, which can be considered as the smallest representative unit of the CNTh product, effectively mirroring the composition of the entire sample. It should contain nine PD-

https://doi.org/10.1021/acs.nanolett.4c04895
Nano Lett. 2025, 25, 1028−1035

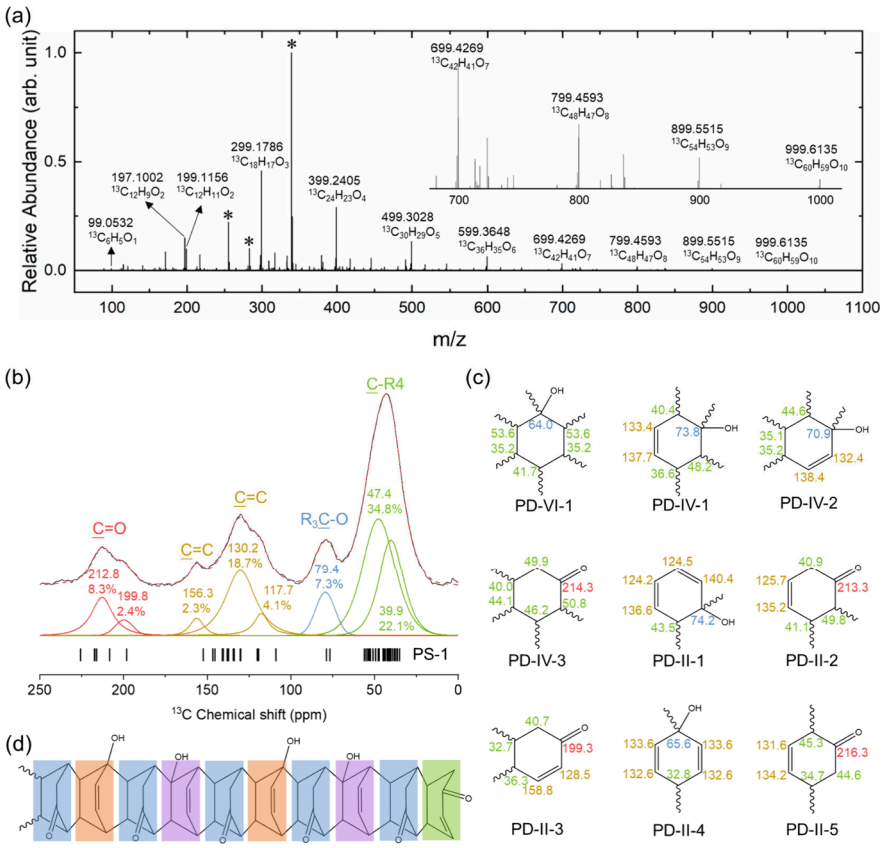

Figure 4. (a) High-resolution mass spectrum of PE-30-$^{13}C_6$. The main column bleed peaks are marked by asterisks. The inset shows the amplified spectrum in the region of m/z = 670−1030. (b) DP ^{13}C ssNMR of PE-30-$^{13}C_6$ with fitted results. The simulated NMR shifts of proposed model PS-1 are shown at the bottom. (c) Simulated ^{13}C chemical shifts of proposed local structures. The chemical shifts are marked with the same colors as the corresponding NMR peaks. (d) Proposed product structure PS-1. The local structures of PD-IV-1, PD-IV-2, PD-IV-3, and PD-II-3 are marked in purple, orange, blue, and green, respectively.

IV units and one PD-II-3 unit based on the peak observed at 156.3 ppm. Considering the proportion of C=O content (10.7%), it suggests there should be six units containing C=O [exp. C=O content/theo. C(O) content × number of units = 0.107/(1/6) × 10 = 6]. As the PD-II-3 carries one C=O, the other five C=O units are attributed to PD-IV-3, while the remaining rings are PD-IV-1 and/or PD-IV-2. Combining these insights, we propose one of the possible product structures (PS-1, Figure 4d), comprising five PD-IV-3, two PD-IV-1, and two PD-IV-2 units, along with one PD-II-3 unit. The simulated NMR results of this proposed structure align well with the experimental results, as shown in Figure 4b. Further confirmation comes from total scattering experiments, where X-ray and neutron total scattering data collected from the PE-30 and deuterated phenol products (PE-30-D_6), respectively, show $G(r)$ plots that align with the simulated structure (Figure 5).

Despite these findings, the precise determination of the intrathread structure remains challenging due to the numerous possible arrangements of the ten chosen units. We simulated four additional candidate models, and although their predicted NMR shifts and PDF data show some differences, these variations are not sufficient to definitively determine the precise arrangement of the structural localization within the nanothreads (Figure S14). As a result, further investigation will be required to fully elucidate the intrathread structure.

Compared to the fully saturated degree-6 CNTh, the partially saturated degree-4 CNTh still shows remarkable

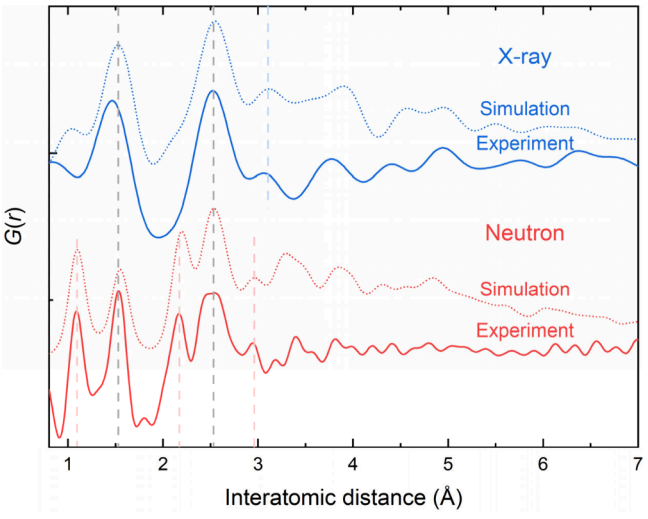

Figure 5. Comparisons between PDF calculated for the proposed PS-1 structure and experiments. The red and blue lines represent neutron and X-ray $G(r)$, respectively, with experimental results depicted as solid lines and simulation results shown as dashed lines.

strength and stiffness, but softer with lower strengths.[29] The remaining unreacted double bonds can tune the band gap, which makes it have wider band gap range (~1.8 eV-4.0 eV) and shows the electronic behavior changes from semiconductor to insulator, while the saturated DNTh usually

https://doi.org/10.1021/acs.nanolett.4c04895
Nano Lett. 2025, 25, 1028−1035

have wide bandgap (>4.0 eV) and can only act as the insulator.[29] For our phenol degree-4 CNTh, it has hydroxyl and carboxyl groups at the surface of the CNThs, which may enhance the interfacial interactions between the CNTh and the polymer matrix.[2] Thus, based on these facts, similar proposed applications for the saturated CNThs can also be expected for these unsaturated CNThs, such as mechanical energy storage device and resonator,[1,36] and the presence of the functional groups in phenol degree-4 CNTh may also make it possible to be used as the fillers in reinforced nanocomposites.[2]

In summary, our investigation into phenol under high pressure revealed two phase transitions occurring below 0.5 and around 4 GPa. Above 20 GPa, phenol polymerized into a degree-4 nanothread through [4 + 2] Diels−Alder reactions, accompanied by the formation of carbon−oxygen double bonds. Quantitative solid-state NMR analysis indicated that approximately 59.4% of the C−OH groups were converted to C=O, likely through a keto−enol tautomerization process, which hindered the formation of degree-6 product. This hydrogen transfer during polymerization highlights the critical role of hydroxyl groups in inhibiting further intracolumn polymerization, thereby serving as a passivating agent under high-pressure conditions. This discovery holds significant implications for designing precursors and manipulating reaction pathways under high pressure, offering valuable insights for future research and applications in nanomaterials.

■ ASSOCIATED CONTENT

Supporting Information

The Supporting Information is available free of charge at https://pubs.acs.org/doi/10.1021/acs.nanolett.4c04895.

Additional data of the in situ Raman, IR, and UV−vis spectra as well as the in situ XRD data of phenol; Rietveld refinement result of phenol-D_6 under high pressure; SEM, XRD pattern, and XPS spectra of PE-30; candidate degree-4 nanothread models and their predicted NMR shifts, as well as calculated PDF data compared with experimental results; assignments of vibration modes of phenol Phase II; lattice parameters of phenol at 1 and 4 GPa; atomic coordinates of phenol at 1 and 4 GPa; observed relative percentages of survey scan and C 1s, O 1s from XPS and fitted results of DP ^{13}C ssNMR (PDF)

■ AUTHOR INFORMATION

Corresponding Author

Kuo Li − *Center for High Pressure Science and Technology Advanced Research, Beijing 100193, P. R. China;* orcid.org/0000-0002-4859-6099; Email: likuo@hpstar.ac.cn

Authors

Xin Yang − *Center for High Pressure Science and Technology Advanced Research, Beijing 100193, P. R. China*

Guangwei Che − *Center for High Pressure Science and Technology Advanced Research, Beijing 100193, P. R. China*

Yajie Wang − *Center for High Pressure Science and Technology Advanced Research, Beijing 100193, P. R. China*

Peijie Zhang − *Center for High Pressure Science and Technology Advanced Research, Beijing 100193, P. R. China;* orcid.org/0000-0001-6355-5482

Xingyu Tang − *Center for High Pressure Science and Technology Advanced Research, Beijing 100193, P. R. China*

Puyi Lang − *Center for High Pressure Science and Technology Advanced Research, Beijing 100193, P. R. China*

Dexiang Gao − *Center for High Pressure Science and Technology Advanced Research, Beijing 100193, P. R. China*

Xuan Wang − *Center for High Pressure Science and Technology Advanced Research, Beijing 100193, P. R. China;* orcid.org/0000-0001-6647-9542

Yida Wang − *Center for High Pressure Science and Technology Advanced Research, Beijing 100193, P. R. China*

Takanori Hattori − *J-PARC Center, Japan Atomic Energy Agency, Tokai, Ibaraki 319-1195, Japan*

Jun Abe − *Neutron Science and Technology Center, Comprehensive Research Organization for Science and Society (CROSS), Tokai, Ibaraki 319-1106, Japan*

Aijiao Guan − *Institute of Chemistry, Chinese Academy of Science, Beijing 100190, P. R. China*

Junfeng Xiang − *Institute of Chemistry, Chinese Academy of Science, Beijing 100190, P. R. China*

Qian Li − *Institute of Chemistry, Chinese Academy of Science, Beijing 100190, P. R. China;* orcid.org/0000-0003-3366-3858

Xiaohuan Lin − *Center for High Pressure Science and Technology Advanced Research, Beijing 100193, P. R. China*

Xiao Dong − *Key Laboratory of Weak-Light Nonlinear Photonics, School of Physics, Nankai University, Tianjin 300071, P. R. China;* orcid.org/0000-0003-4533-1914

Ho-kwang Mao − *Center for High Pressure Science and Technology Advanced Research, Beijing 100193, P. R. China; Shanghai Key Laboratory MFree, Shanghai Advanced Research in Physical Sciences, Shanghai 201203, P. R. China*

Haiyan Zheng − *Center for High Pressure Science and Technology Advanced Research, Beijing 100193, P. R. China;* orcid.org/0000-0002-4727-5912

Complete contact information is available at: https://pubs.acs.org/10.1021/acs.nanolett.4c04895

Author Contributions

The manuscript was written through contributions of all authors. All authors have given approval to the final version of the manuscript.

Notes

The authors declare no competing financial interest.

■ ACKNOWLEDGMENTS

The authors acknowledge the support of the National Key Research and Development Program of China (Grant No. 2023YFA1406200), National Natural Science Foundation of China (Grant No. 22022101). The synchrotron X-ray diffraction was carried out with the support of 4W2 beamline of Beijing Synchrotron Radiation Facility (BSRF) and 15U at Shanghai Synchrotron Radiation Facility (SSRF). The synchrotron X-ray total scattering was performed at 13HB beamlines at Shanghai Synchrotron Radiation Facility (SSRF). The neutron diffraction experiment was conducted under J-PARC MLF user program (Proposal No. 2020B0450). This study was partially supported by Synergic Extreme Condition User Facility (SECUF) and "Fenghuang" diffractometer of China Mianyang Research Reactor (CMRR). The authors thank Dr. Leiming Fang for supporting neutron diffraction measurements. The authors thank Dr. Xuewang Gao and Dr.

https://doi.org/10.1021/acs.nanolett.4c04895
Nano Lett. 2025, 25, 1028−1035

Yehua Han for supporting the electron spray ionization mass spectrometry measurements. The authors thank Dr. Xujie Lv for supporting the in situ UV−vis measurements.

REFERENCES

(1) Duan, K.; Li, Y.; Li, L.; Hu, Y.; Wang, X. Diamond nanothreads based resonators: ultrahigh sensitivity and low dissipation. *Nanoscale* **2018**, *10* (17), 8058−8065.
(2) Zhan, H.; Zhang, G.; Tan, V. B. C.; Cheng, Y.; Bell, J. M.; Zhang, Y.-W.; Gu, Y. Diamond nanothread as a new reinforcement for nanocomposites. *Adv. Funct. Mater.* **2016**, *26* (29), 5279−5283.
(3) Fitzgibbons, T. C.; Guthrie, M.; Xu, E. S.; Crespi, V. H.; Davidowski, S. K.; Cody, G. D.; Alem, N.; Badding, J. V. Benzene-derived carbon nanothreads. *Nat. Mater.* **2015**, *14* (1), 43−47.
(4) Stojkovic, D.; Zhang, P.; Crespi, V. H. Smallest nanotube: breaking the symmetry of sp^3 bonds in tubular geometries. *Phys. Rev. Lett.* **2001**, *87* (12), 125502.
(5) Wen, X. D.; Hoffmann, R.; Ashcroft, N. W. Benzene under high pressure: a story of molecular crystals transforming to saturated networks, with a possible intermediate metallic phase. *J. Am. Chem. Soc.* **2011**, *133* (23), 9023−9035.
(6) Barua, S. R.; Quanz, H.; Olbrich, M.; Schreiner, P. R.; Trauner, D.; Allen, W. D. Polytwistane. *Chem.—Eur. J.* **2014**, *20* (6), 1638−1645.
(7) Chen, B.; Hoffmann, R.; Ashcroft, N. W.; Badding, J.; Xu, E.; Crespi, V. Linearly polymerized benzene arrays as intermediates, tracing pathways to carbon nanothreads. *J. Am. Chem. Soc.* **2015**, *137* (45), 14373−14386.
(8) Zhao, W.; Zhang, J.; Sun, Z.; Xiao, G.; Zheng, H.; Li, K.; Li, M.; Zou, B. Chemical synthesis driven by high pressure. *CCS Chem.* **2025**, Just Accepted. DOI: 10.31635/ccschem.025.202405293.
(9) Huss, S.; Wu, S.; Chen, B.; Wang, T.; Gerthoffer, M. C.; Ryan, D. J.; Smith, S. E.; Crespi, V. H.; Badding, J. V.; Elacqua, E. Scalable synthesis of crystalline one-dimensional carbon nanothreads through modest-pressure polymerization of furan. *ACS Nano* **2021**, *15* (3), 4134−4143.
(10) Matsuura, B. S.; Huss, S.; Zheng, Z.; Yuan, S.; Wang, T.; Chen, B.; Badding, J. V.; Trauner, D.; Elacqua, E.; van Duin, A. C. T.; Crespi, V. H.; Schmidt-Rohr, K. Perfect and defective ^{13}C-furan-derived nanothreads from modest-pressure synthesis analyzed by ^{13}C NMR. *J. Am. Chem. Soc.* **2021**, *143* (25), 9529−9542.
(11) Wang, X.; Yang, X.; Wang, Y.; Tang, X.; Zheng, H.; Zhang, P.; Gao, D.; Che, G.; Wang, Z.; Guan, A.; Xiang, J. F.; Tang, M.; Dong, X.; Li, K.; Mao, H. K. From biomass to functional crystalline diamond nanothread: pressure-induced polymerization of 2,5-furandicarboxylic acid. *J. Am. Chem. Soc.* **2022**, *144* (48), 21837−21842.
(12) Dunning, S. G.; Chen, B.; Zhu, L.; Cody, G. D.; Chariton, S.; Prakapenka, V. B.; Zhang, D.; Strobel, T. A. Synthesis and post-processing of chemically homogeneous nanothreads from 2,5-furandicarboxylic acid. *Angew. Chem., Int. Ed.* **2023**, *62* (14), No. e202217023.
(13) Gao, D.; Tang, X.; Xu, J.; Yang, X.; Zhang, P.; Che, G.; Wang, Y.; Chen, Y.; Gao, X.; Dong, X.; Zheng, H.; Li, K.; Mao, H. K. Crystalline $C_3N_3H_3$ tube (3,0) nanothreads. *Proc. Natl. Acad. Sci. U. S. A.* **2022**, *119* (17), No. e2201165119.
(14) Biswas, A.; Ward, M. D.; Wang, T.; Zhu, L.; Huang, H. T.; Badding, J. V.; Crespi, V. H.; Strobel, T. A. Evidence for orientational order in nanothreads derived from thiophene. *J. Phys. Chem. Lett.* **2019**, *10* (22), 7164−7171.
(15) Dunning, S. G.; Zhu, L.; Chen, B.; Chariton, S.; Prakapenka, V. B.; Somayazulu, M.; Strobel, T. A. Solid-state pathway control via reaction-directing heteroatoms: ordered pyridazine nanothreads through selective cycloaddition. *J. Am. Chem. Soc.* **2022**, *144* (5), 2073−2078.
(16) Li, Y.; Tang, X.; Zhang, P.; Wang, Y.; Yang, X.; Wang, X.; Li, K.; Wang, Y.; Wu, N.; Tang, M.; Xiang, J.; Lin, X.; Lee, H. H.; Dong, X.; Zheng, H.; Mao, H. K. Scalable high-pressure synthesis of sp^2-sp^3 carbon nanoribbon via [4 + 2] polymerization of 1,3,5-triethynylbenzene. *J. Phys. Chem. Lett.* **2021**, *12* (30), 7140−7145.
(17) Fei, Y.; Li, Y.; Lang, P.; Tang, X.; Zhang, P.; Che, G.; Dong, X.; Li, K.; Zheng, H. High pressure polymerization of 2,6-diethynylpyridine. *J. Phys. Chem. C* **2024**, *128* (17), 7286−7293.
(18) Tang, W. S.; Strobel, T. A. Evidence for functionalized carbon nanothreads from π-stacked, para-disubstituted benzenes. *J. Phys. Chem. C* **2020**, *124* (45), 25062−25070.
(19) Ward, M. D.; Tang, W. S.; Zhu, L.; Popov, D.; Cody, G. D.; Strobel, T. A. Controlled single-crystalline polymerization of $C_{10}H_8$·$C_{10}F_8$ under pressure. *Macromolecules* **2019**, *52* (20), 7557−7563.
(20) Friedrich, A.; Collings, I. E.; Dziubek, K. F.; Fanetti, S.; Radacki, K.; Ruiz-Fuertes, J.; Pellicer-Porres, J.; Hanfland, M.; Sieh, D.; Bini, R.; Clark, S. J.; Marder, T. B. Pressure-induced polymerization of polycyclic arene-perfluoroarene cocrystals: single crystal X-ray diffraction studies, reaction kinetics, and design of columnar hydrofluorocarbons. *J. Am. Chem. Soc.* **2020**, *142* (44), 18907−18923.
(21) Gerthoffer, M. C.; Wu, S.; Chen, B.; Wang, T.; Huss, S.; Oburn, S. M.; Crespi, V. H.; Badding, J. V.; Elacqua, E. 'Sacrificial' supramolecular assembly and pressure-induced polymerization: toward sequence-defined functionalized nanothreads. *Chem. Sci.* **2020**, *11* (42), 11419−11424.
(22) Wang, Y.; Dong, X.; Tang, X.; Zheng, H.; Li, K.; Lin, X.; Fang, L.; Sun, G.; Chen, X.; Xie, L.; Bull, C. L.; Funnell, N. P.; Hattori, T.; Furukawa, A. S.; Chen, J.; Hensley, D. K.; Cody, G. D.; Ren, Y.; Lee, H. H.; Mao, H. Pressure-induced Diels−Alder reactions in C_6H_6-C_6F_6 cocrystal towards graphane structure. *Angew. Chem., Int. Ed.* **2019**, *58* (5), 1468−1473.
(23) Nobrega, M. M.; Temperini, M. L. A.; Bini, R. Probing the chemical stability of aniline under high pressure. *J. Phys. Chem. C* **2017**, *121* (13), 7495−7501.
(24) Nobrega, M. M.; Teixeira-Neto, E.; Cairns, A. B.; Temperini, M. L. A.; Bini, R. One-dimensional diamondoid polyaniline-like nanothreads from compressed crystal aniline. *Chem. Sci.* **2018**, *9* (1), 254−260.
(25) Allan, D. R.; Clark, S. J.; Dawson, A.; McGregora, P. A.; Parsonsc, S. Pressure-induced polymorphism in phenol. *Acta Crystallogr. B* **2002**, *58* (6), 1018−1024.
(26) Gerthoffer, M. C.; Xu, B.; Wu, S.; Cox, J.; Huss, S.; Oburn, S. M.; Lopez, S. A.; Crespi, V. H.; Badding, J. V.; Elacqua, E. Mechanistic insights into the pressure-induced polymerization of aryl/perfluoroaryl co-crystals. *Polym. Chem.-UK* **2022**, *13* (10), 1359−1368.
(27) Ciabini, L.; Santoro, M.; Bini, R.; Schettino, V. High pressure photoinduced ring opening of benzene. *Phys. Rev. Lett.* **2002**, *88* (8), No. 085505.
(28) Sussardi, A. N.; Turner, G. F.; Richardson, J. G.; Spackman, M. A.; Turley, A. T.; McGonigal, P. R.; Jones, A. C.; Moggach, S. A. Tandem high-pressure crystallography-optical spectroscopy unpacks noncovalent interactions of piezochromic fluorescent molecular rotors. *J. Am. Chem. Soc.* **2023**, *145* (36), 19780−19789.
(29) Demingos, P. G.; Muniz, A. R. Electronic and mechanical properties of partially saturated carbon and carbon nitride nanothreads. *J. Phys. Chem. C* **2019**, *123* (6), 3886−3891.
(30) Vinet, P.; Ferrante, J.; Smith, J. R.; Rose, J. H. A universal equation of state for solids. *J. Phys. C: Solid State Phys.* **1986**, *19* (20), L467.
(31) Li, X.; Baldini, M.; Wang, T.; Chen, B.; Xu, E. S.; Vermilyea, B.; Crespi, V. H.; Hoffmann, R.; Molaison, J. J.; Tulk, C. A.; Guthrie, M.; Sinogeikin, S.; Badding, J. V. Mechanochemical synthesis of carbon nanothread single crystals. *J. Am. Chem. Soc.* **2017**, *139* (45), 16343−16349.
(32) El Hariri El Nokab, M.; Habib, M. H.; Alassmy, Y. A.; Abduljawad, M. M.; Alshamrani, K. M.; Sebakhy, K. O. Solid state NMR a powerful technique for investigating sustainable/renewable cellulose-based materials. *Polymers* **2022**, *14* (5), 1049.
(33) Idström, A.; Schantz, S.; Sundberg, J.; Chmelka, B. F.; Gatenholm, P.; Nordstierna, L. ^{13}C NMR assignments of regenerated

cellulose from solid-state 2D NMR spectroscopy. *Carbohydr. Polym.* **2016**, *151*, 480−487.
(34) Zuckerstätter, G.; Terinte, N.; Sixta, H.; Schuster, K. C. Novel insight into cellulose supramolecular structure through ^{13}C CP-MAS NMR spectroscopy and paramagnetic relaxation enhancement. *Carbohydr. Polym.* **2013**, *93*, 122−128.
(35) Duan, P.; Li, X.; Wang, T.; Chen, B.; Juhl, S. J.; Koeplinger, D.; Crespi, V. H.; Badding, J. V.; Schmidt-Rohr, K. The chemical structure of carbon nanothreads analyzed by advanced solid-state NMR. *J. Am. Chem. Soc.* **2018**, *140* (24), 7658−7666.
(36) Zhan, H.; Zhang, G.; Bell, J. M.; Tan, V. B. C.; Gu, Y. High density mechanical energy storage with carbon nanothread bundle. *Nat. Commun.* **2020**, *11*, 1905.

https://doi.org/10.1021/acs.nanolett.4c04895
Nano Lett. 2025, 25, 1028−1035